Matched boundary layers in turbulent Rayleigh-Bénard convection of mercury

Takehiko Segawa, Antoine Naert, and Masaki Sano
Research Institute of Electrical Communication, Tohoku University, Sendai 980-77, Japan
(Received 2 September 1997)

We analyzed temperature time series recorded in different positions across the boundary layers of a Rayleigh-Bénard convection cell using mercury (Pr=0.024) for Rayleigh numbers (Ra) ranging from 10^6 to 10^8. In the whole range of Ra, several nondimensional quantities have unique, Ra-invariant profiles, if distance is normalized by the thermal boundary layer thickness. This indicates an asymptotic regime of thermal turbulence in which two boundary layers are coupled. Skewness and its time derivative of thermal fluctuations reveal that temperature fluctuations are not buoyancy driven but passively swept by the mean circulation in most of the cell. [S1063-651X(98)06401-0]

PACS number(s): 47.20.Lz, 47.27.Te

The understanding of convective heat transport by a turbulent flow at very high Rayleigh number is of great practical as well as fundamental interest. An important goal is to identify and characterize, if it exists, the ultimate regime of high Rayleigh number thermal turbulence. We chose a Rayleigh-Bénard experiment, that can exhibit the main basic features of hard turbulence in a simple geometry, and well controlled conditions.

In the late 1980s, the pioneering experimental work of Libchaber and co-workers on Rayleigh-Bénard thermal convection revealed a regime of turbulence called ''hard turbulence'' [1–5]. Using helium gas at low temperature allowed them to explore a wide range of Rayleigh number (Ra), the control parameter of the system. The histograms of temperature fluctuations show an exponential-like long tail in the center region of the cell. Since then, though a large number of experimental and theoretical contributions has been done, several open questions remain. An important and quite peculiar point is the existence of a large scale, stable mean flow in the cell. The origin of this flow is still unclear, but it obviously strongly affects the heat transport across the cell by causing a strong wind along the thermally active plates. As the velocity vanishes on the sides of the cell, a viscous boundary layer is created. Therefore, viscous boundary layers coexist along the hot and cold plate with the thermal one, where the temperature drop occurs. The structure of these two layers is a key point to understand heat transfer properties of hard turbulence.

The boundary layers have been carefully investigated experimentally by Belmonte *et al.* in pressurized gas (SF_6) and water, by measuring the temperature fluctuations with a movable probe [6]. They showed the existence of buoyancy driven structure, plumes, transporting heat to the bulk region through the boundary layers. They measured two length scales, λ_T and λ_v, corresponding respectively to the thickness of the thermal and viscous boundary layers. Over the whole range $10^6<\mathrm{Ra}<10^{12}$ accessible to their measurement, λ_v was found larger than λ_T. However, they showed that λ_v decreases faster with increasing Ra than λ_T, at high Ra. Therefore, the two boundary layers are expected to match or cross around at $\mathrm{Ra}\sim 10^{14}$ (for the Prandtl number Pr=0.7). Thus the hard turbulence observed in SF_6, He, or water experiments is not the ultimate one.

The lower the Prandtl number, the smaller the ratio of the boundary layer thicknesses, λ_v/λ_T. The Rayleigh number for this matching is expected to be $\mathrm{Ra}\sim 10^5$ in liquid Hg (Pr =0.024) [7]. It is thus convenient to study in Hg a turbulent regime, otherwise difficult to realize in well controlled experimental conditions in higher Pr fluid.

In this paper, we describe some statistical properties of temperature fluctuations in the upper (cold) boundary layer region of the cell. We show that the profile of several statistical quantities, such as mean, standard deviation, skewness S, flatness F, and the skewness of the time derivative S' of the temperature fluctuations, are independent of Ra if plotted versus the nondimensional distance to the plate: z/λ_T. In our Hg experiment, $S'S$ was observed to be negative outside the viscous boundary layer, implying that the temperature fluctuations are not buoyancy driven but passively swept by the mean flow. The viscous boundary layer thickness evaluated by the shifting power spectrum of temperature fluctuations also has a unique maximum at the Ra invariant z/λ_T. This is evidence that λ_v/λ_T is constant and only one length scale remains: the thermal and viscous boundary layers are coupled.

Our experimental setup is a Rayleigh-Bénard convection cell, a vertical cylinder 10 cm in height and 10 cm in diameter (aspect ratio 1), filled with mercury (for details, see [8,9]). The accessible range of Rayleigh number is $10^6<\mathrm{Ra}<10^8$. The bottom plate is heated by a resistor at constant power, and the top plate is cooled by water circulation. The temperature of the cooling water is regulated by a refrigerator. The rms temperature fluctuations in the plates, for the typical heating power, is 1% of the total temperature difference, $\Delta T\simeq 10\,^\circ\mathrm{C}$, when 100 W power is supplied to the bottom plate.

The temperature in the flow is measured by two 300 μm diameter thermistors, suspended on a 0.8 mm diameter frame. This frame is moved vertically along the center line of the cell by a stepping motor located outside the cell. As the two thermistors are precisely placed at any positions in the upper half of the cell, we can investigate the structures near the cooled top plate in detail. Temperature fluctuations are measured through an ac capacitance bridge with a lock-in amplifier (PAR124A). The signal is digitized with a 13 bit resolution digital spectrum analyzer (HP3563A) at sampling

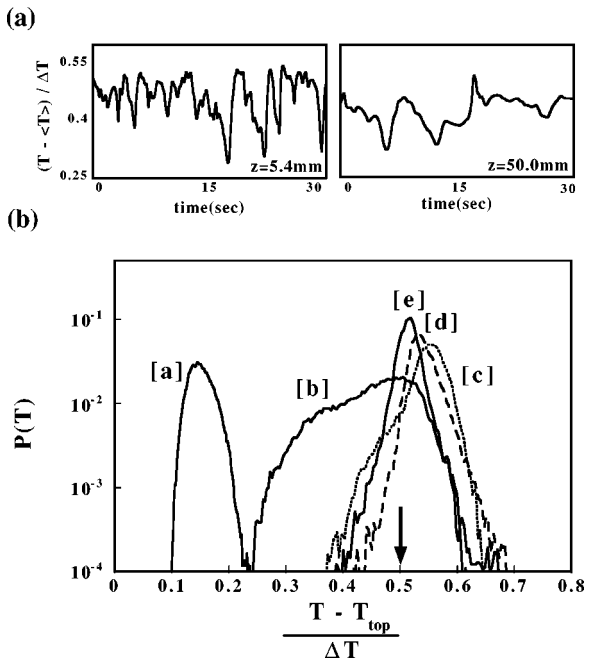

FIG. 1. (a) The time series of temperature near the boundary layers and at the center for Ra$=3.5\times10^7$, here $\lambda_T=4.2$ mm and $\lambda_v=2.5$ mm. The temperature fluctuations are normalized by the temperature difference, ΔT. (b) Histograms of temperature fluctuations, normalized by ΔT and mean temperature of the top plate $T_{\rm top}$, at various heights for Ra$=3.5\times10^7$. The heights are (a) $z=$ 1.1 mm, (b) 5.4 mm, (c) 16.6 mm, (d) 36 mm, and (e) 50 mm. The arrow points $\Delta T/2$.

frequency ranging from 5 to 26 Hz. Over 50 000 data points are measured for each time series.

We measured a temperature signal at different distances z from the top plate, for different values of Ra. Samples of temperature signal in the boundary layers region and at the center of the cell, and a few histograms are plotted in Fig. 1. Temperature is Gaussian near the plate. In the center, the histogram shows exponential-like tails, a common character of hard turbulence. In intermediate regions, the shape changes, due to large low temperature excursions. To characterize the evolution of those histograms, we calculated the moments: the mean $\langle T\rangle$, the standard deviation $\langle(T-\langle T\rangle)^2\rangle^{1/2}$, and the nondimensional third and fourth order moments: the skewness S and flatness F, defined as

$$S=\frac{\langle(T-\langle T\rangle)^3\rangle}{\langle(T-\langle T\rangle)^2\rangle^{3/2}}, \tag{1}$$

$$F=\frac{\langle(T-\langle T\rangle)^4\rangle}{\langle(T-\langle T\rangle)^2\rangle^{2}}. \tag{2}$$

S characterizes the asymmetry of the distribution. Note that negative (positive) skewness corresponds to an asymmetry toward colder (warmer) temperatures. F is useful to characterize large deviations of fluctuations. For instance, Gaussian distribution corresponds to $F=3$, and exponential distribution to $F=6$.

The boundary layer thickness λ_T has been obtained in a previous work [8], from the best fit of the profile $\langle T\rangle$ with a

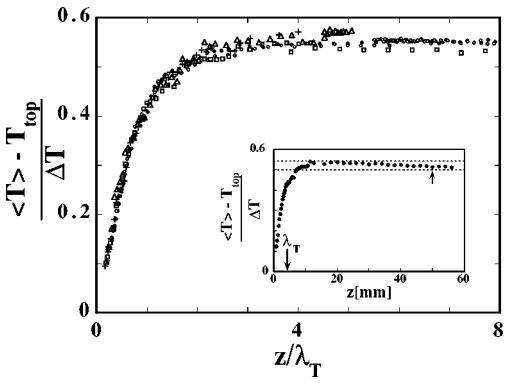

FIG. 2. Temperature profiles normalized by $T_{\rm top}$ and ΔT near the top plate as a function of z/λ_T for Ra: (●) 8.0×10^7, (○) 6.1×10^7, (□) 3.5×10^7, (△) 2.0×10^7, and (+) 6.0×10^6. Inset shows the temperature inversion, which is estimated about 10% of total temperature difference ΔT around the center for Ra$=3.5\times10^7$.

convenient function (hyperbolic tangent) of the nondimensional variable: z/λ_T. At this distance λ_T, the standard deviation $\langle(T-\langle T\rangle)^2\rangle^{1/2}$ happens to be maximum, giving another way to evaluate the boundary layer thickness.

In Fig. 2, one can see the profiles of nondimensional $\langle T\rangle$, versus z/λ_T for several Ra. These profiles nicely collapse to a unique curve, independently of Ra. In Figs. 3 and 4, one can see that S and F have unique profiles as well. This feature is different from the case of pressurized SF_6 (Pr$=0.7$), as can be seen in the Fig. 3 of Ref. [6]. We note that the mean temperature profile is slightly inverted in the central region of the cell ($d\langle T\rangle/dz>0$), indicating a stable stratification of the fluid. Temperature inversion is about 10% of the total temperature difference ΔT. Since the typical fluctuations in the center is 3% of ΔT, buoyancy force is not dominant.

We also plotted the skewness of the temperature time derivative, defined as

$$S'=\frac{\langle(dT/dt)^3\rangle}{\langle(dT/dt)^2\rangle^{3/2}}, \tag{3}$$

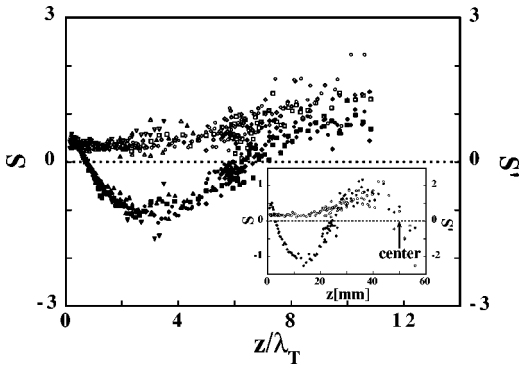

FIG. 3. Overlap of several profiles; the skewness S (solid symbols) and the skewness of time derivative S' (open symbols) of temperature fluctuations as a function of the distance z/λ_T for Ra: (□) 8.0×10^7, (◇) 6.1×10^7, (○) 3.5×10^7, (△) 2.0×10^7, and (▽) 3.0×10^6. Inset shows S and S' as a function of z from the top plate for Ra$=3.5\times10^7$.

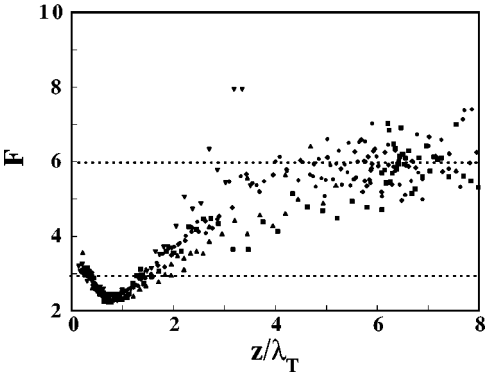

FIG. 4. The flatness of temperature fluctuations F versus the distance z/λ_T. The symbols are the same as in Fig. 3. Horizontal lines denotes $F=3$ and $F=6$. They correspond to the values expected for Gaussian and exponential distribution, respectively.

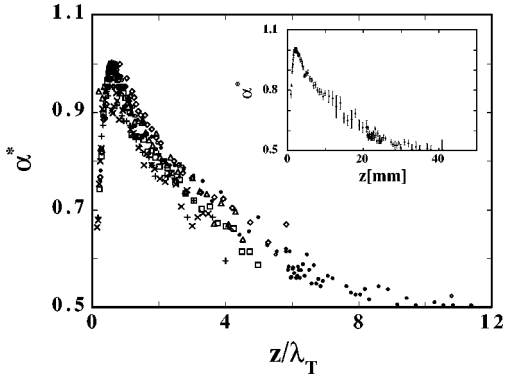

FIG. 5. The frequency shift α^* as a function of z/λ_v for Ra: (●) 8.0×10^7, (○) 6.1×10^7, (□) 3.5×10^7, (◇) 2.9×10^7, (△) 2.0×10^7, (+) 6.0×10^6, and (×) 3.0×10^6. Inset shows α^* with error bar as a function of the distance z from the top plate for Ra $=8.0\times10^7$. The viscous boundary layer thickness is the position at which α^* reaches its maximum.

where

$$\frac{dT}{dt}=T_{i+1}-T_i \tag{4}$$

in Fig. 3. S' characterizes an asymmetry of derivatives of the signal. If buoyancy-driven structures (plumes) exist near the cold boundary layer, excursion away from the mean (cooling) is followed by a less rapid return (warming). The former contributes to a decrease in S' while the latter contributes to an increase. As an outcome, cold plumes result in negative S'.

However, we observed that S' is positive from the top (cold) plate to the center in this experiment (see Fig. 3). This character is very different from that of hard turbulence [13]. Note also that S' curves have a unique profile.

These quantities have been measured by other authors in the boundary layer of a slightly heated or cooled surface, where temperature is passively mixed by the turbulent flow [10,11]. Along a heated plate, $S'<0$ and $S>0$, whereas $S'>0$ and $S<0$ was observed along a cooled plate. Therefore, $S'S<0$ in the case of a passive scalar. The opposite sign has been found in SF_6 gas hard turbulence convection: $S'S>0$ ($S<0$,$S'<0$), outside the thermal boundary layers of the top plate [12]. This feature was explained by the existence of active thermal structures driven by buoyancy, plumes, which were observed in a water experiment [13]. In the present situation, we found that $SS'<0$ outside of viscous boundary layer as shown in Fig. 3. In fact, the sign of $S'S$ defines three distinct regions, as can be seen in Fig. 3. Inside the viscous boundary layer, $S'S>0$. From $z/\lambda_T=\lambda_v/\lambda_T\simeq0.6$ to about 6, $S'S<0$. In the central region, of stable temperature stratification, $S'S>0$. However, in this region where the mean velocity is small or null, $S'S>0$ may not imply that buoyancy is dominant. Actually, there are several indications of the passive character of temperature fluctuations in the central region of the cell, in low Pr hard turbulence [8,14]. The mean, large scale flow is driven by buoyancy only within a thin layer along the walls, the viscous boundary layer, where $S'S>0$. Outside of viscous layer, plumes are not active. The turbulence in the rest of the cell is energy fed by the shear along the boundary layer, mixing temperature as a passive scalar.

Due to the high thermal conductivity of Hg and the large fluctuations of temperature in thermal turbulence, a direct measurement of the velocity fluctuations is difficult. In recent studies, we used an indirect method developed by Belmonte *et al.* to evaluate the viscous boundary layer thickness, λ_v [6,8,13]. Because the highest frequencies of the temperature fluctuations are due to the advection of the smallest ''thermal structures'' by the mean flow, the highest frequency has to be higher where the mean flow is faster. The viscous boundary layer thickness λ_v is defined as the distance to the plate where this maximum occurs. This method relies on the assumption that the size of the smallest thermal structures does not change too much in this boundary layer region. The highest frequency was determined as the frequency at which the power spectrum reaches the background noise level.

In this paper we developed a reliable method to evaluate the highest frequency of the signal. For each value of Ra, the power spectrum of temperature $P_z(f)$ at the distances z are shifted on the frequency axis to fit a reference spectrum $P_{z_0}(f)$, minimizing the quantity

$$Er(\alpha)=\frac{1}{f_c-f_H}\int_{f_H}^{f_c}\left[\ln\frac{P_z(\alpha f)}{P_{z_0}(f)}\right]^2 df, \tag{5}$$

where f_H is the frequency at which the level of $P_{z_0}(f)$ becomes a fixed value P_0 and f_c is the cutoff frequency at which it sinks into noise level.

The value α^* for which Er takes a minimum is the ratio of characteristic high frequencies of the two spectra. The reference spectrum $P_{z_0}(f)$ is a power spectrum at an arbitrary distance z_0. We chose z_0 where the spectrum has the maximum f_c. Therefore, the maximum value of the best fit parameter α^* is 1 at $z\simeq\lambda_v$. The lower cutoff, f_H, was varied by changing P_0 from -45 to -80 dB, but α^* did not change. The nondimensional profile of the characteristic frequency, α^*, is plotted in Fig. 5 versus z/λ_T for several Ra. The position of the maximum of α^* does not depend on Ra. Thus the ratio of two length scales is constant: λ_v/λ_T

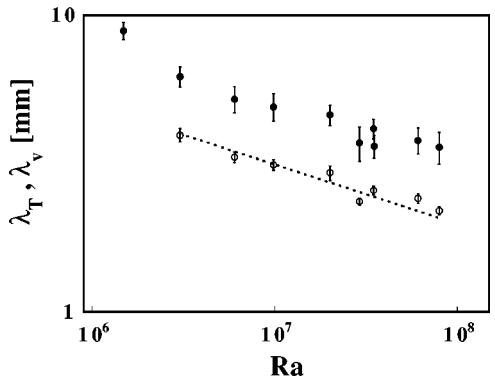

FIG. 6. Thickness of the thermal and viscous boundary layers as a function of Ra. λ_v (○) is evaluated by shifting power spectrum of temperature fluctuations. λ_T (●) is determined by the position of the maximum rms fluctuations [9]. The dashed line shows the slope -0.20 for comparison.

$=0.63\pm0.05$. In the range of Ra investigated here, the two boundary layers are coupled as shown in Fig. 6.

We may have reached in our Hg experiment the ultimate regime of hard turbulence which was expected to result from the matching of the two layers. In a previous article [9], we have shown from the same data set $\lambda_T \propto \mathrm{Ra}^{-0.20\pm0.02}$, which is significantly different from the scaling relation expected if the boundary layer is laminar (diffusion limited): $\lambda_T \propto 1/\mathrm{Nu} \propto \mathrm{Ra}^{-0.25\pm0.005}$. If two boundary layers are matched, the thermal boundary layer is no longer diffusion limited. In that case, two exponents need not be the same. The regime of matched boundary layers is expected to exhibit different statistical properties than that seen at lower Rayleigh number. In fact we observed the new regime and showed peculiar statistical properties of boundary layer, i.e., $S'S<0$. That corresponds to the absence of plumes. We hope these observations will motivate further experimental or numerical investigations, and the construction of a consistent and global theoretical picture of thermal hard turbulence.

We are grateful to M. Sugawara for building the experimental cell and to J. A. Glazier, A. Belmonte, Y. Sawada, S. Cioni, S. Ciliberto, and B. Castaing for stimulating discussions. This work was supported by the Japanese Grant-in-Aid for Science Research Fund from Ministry of Education, Science and Culture (No. 08454104 and 09440146). A. N. acknowledges support from the EC/JSPS joint fellowship program and the warm hospitality of Tohoku University.

[1] F. Heslot, B. Castaing, and A. Libchaber, Phys. Rev. A **36**, 5870 (1987).
[2] B. Castaing, G. Gunaratne, F. Heslot, L. Kadanoff, A. Libchaber, S. Thomae, X. Z. Wu, G. Zaleski, and G. Zanetti, J. Fluid Mech. **204**, 1 (1989).
[3] M. Sano, X. Z. Wu, and A. Libchaber, Phys. Rev. A **40**, 6421 (1989); X. Z. Wu and A. Libchaber, *ibid.* **45**, 842 (1992).
[4] X. Z. Wu, L. Kadanoff, A. Libchaber, and M. Sano, Phys. Rev. Lett. **64**, 2140 (1990).
[5] T. H. Solomon and J. P. Gollub, Phys. Rev. Lett. **64**, 2382 (1990); Phys. Rev. A **43**, 6683 (1991).
[6] A. Belmonte, A. Tilgner, and A. Libchaber, Phys. Rev. Lett. **70**, 4067 (1993).
[7] S. Cioni, S. Ciliberto, and J. Sommeria, J. Fluid Mech. **335**, 11 (1996).
[8] T. Takeshita, T. Segawa, J. G. Glazier, and M. Sano, Phys. Rev. Lett. **76**, 1465 (1996).
[9] A. Naert, T. Segawa, and M. Sano, Phys. Rev. E **56**, 1302 (1997).
[10] K. Sreenivasan, R. Antonia, and H. Danh, Phys. Fluids **20**, 1238 (1977).
[11] P. Mestayer, J. Fluid Mech. **125**, 475 (1982).
[12] A. Belmonte and A. Libchaber, Phys. Rev. E **53**, 4893 (1996).
[13] A. Belmonte, A. Tilgner, and A. Libchaber, Phys. Rev. E **50**, 269 (1994).
[14] S. Cioni, S. Ciliberto, and J. Sommeria, Europhys. Lett. **32**, 413 (1995).